State Estimation of Doubly Fed Induction Generator Wind Turbine in Complex Power Systems

Shenglong Yu, *Student Member, IEEE*, Kianoush Emami, *Member, IEEE*, Tyrone Fernando, *Senior Member, IEEE*, Herbert H. C. Iu, *Senior Member, IEEE*, and Kit Po Wong, *Fellow, IEEE*

***Abstract*—This paper presents a general framework for the doubly fed induction generator connected to a complex power system in order to facilitate the dynamic estimation of its states using noisy PMU measurements. State estimation considering the whole power system with the occurrence of electric faults is performed using the Unscented Kalman Filter (UKF) with a bad data detection scheme. Such a state estimation scheme for a DFIG is important because not all dynamic states of a DFIG are easily measurable. Furthermore, the proposed state estimation technique is decentralized and the network topology of the entire power system is taken into consideration in the estimation process. In order to enhance the error tolerance and self-correction of the power system, bad data detection technique is implemented. A performance comparison with Extended Kalman Filter (EKF) is also discussed.**

***Index Terms*—Bad data detection, doubly fed induction generator (DFIG), EKF, PMU, state estimation, UKF.**

I. Introduction

With the depletion of fossil fuel reservoir, wind power as a clean and renewable energy source has attracted a lot of attention in recent decades. DFIGs are now one of the most commonly used wind power generators in the industry [1]. Mathematical modelling and various control strategies are reported in [2]–[4]. In the power electronics field, a great contribution has been made to the converters and inverters used in DFIG [5]. Further studies on DFIG such as eigenvalue sensitivity analysis and fault ride through can be found in [6], [7]. Most recent studies that have been done in control design of DFIG and Power System Stabilizer (PSS) application to DFIG are presented in [8], [9]. Nevertheless, there has been no reported work on the dynamic state estimation of DFIG, which is the subject of this paper. UKF and EKF estimation schemes to dynamically estimate the states of a DFIG connected to a complex power system using PMU measurements are presented in this paper.

Manuscript received August 14, 2015; revised November 18, 2015; accepted December 08, 2015. Date of publication January 18, 2016; date of current version October 18, 2016. Paper no. TPWRS-01147-2015.

The authors are with the School of Electrical, Electronic and Computer Engineering, The University of Western Australia, Crawley WA 6009, Australia (e-mail: shenglong.yu@research.uwa.edu.au; kianoush.emami@research.uwa.edu.au; tyrone.fernando@uwa.edu.au; herbert.iu@uwa.edu.au; kitpo.wong@uwa.edu.au).

Color versions of one or more of the figures in this paper are available online at http://ieeexplore.ieee.org.

Digital Object Identifier 10.1109/TPWRS.2015.2507620

State estimation for complex power systems is a piece of indispensable work in the investigation of power systems because of the need of controller designs and the unavailability of some states. The dynamic state estimation of synchronous generators are widely reported in the literature, see [10]–[13] and references therein. Those reported estimation schemes for synchronous generators are primarily based on Kalman filter techniques. Likewise, on a similar front, we report UKF and EKF based techniques for estimating the dynamic states of DFIG. The dynamic state estimation of DFIG is challenging due to the high nonlinearity of DFIG and the wide range of operating points [14]. Moreover, the equivalent circuit of the DFIG is more complicated than that of the synchronous generator due to the doubly fed connection via the rotor side and the grid side controllers. The estimation must be performed considering the overall power system network, which leads to the result that any change in the network will have an impact on the performance of DFIG and vice versa. The proposed estimation scheme in this paper, however, is decentralized and can be obtained by only observing and processing local data. With the increased popularity of UKF and EKF as two main methods to estimate states and their mature applicability, using them to estimate states in DFIG is feasible and practicable. A good summary of UKF estimating nonlinear states is shown in [15]. EKF is commonly used to estimate nonlinear system with linearized system parameters and has already been considered as a standard theory of state estimations and navigation systems [16]. The main drawback of EKF, nonetheless, is the fact that when the system is highly nonlinear, it will produce unsatisfactory results and consequently, UKF shall generate a better result than EKF when estimating dynamic states of nonlinear systems. In this paper, UKF will be used as a main method for state estimation while EKF will be implemented as a comparison method.

Phasor Measurement Units (PMUs) have witnessed its significant developments in recent years and are now widely used in power distribution and power system infrastructure [17]. PMUs can provide and send measurement data at a sampling rate of 48 samples per cycle (2880 samples/s for 60 Hz systems) [18], which displays a significant advantage in dealing with nonlinear state estimation as data collected at such fast rate will accurately reflect and effectively track the change trend of nonlinear states. Bad data detection will also be incorporated into UKF to eliminate unwanted data.

In this paper, we consider the mathematical model of a DFIG and formulate it in a manner that can be incorporated with UKF and EKF filtering algorithms. In particular, the dynamics of the electrical network is considered to respond a lot faster than

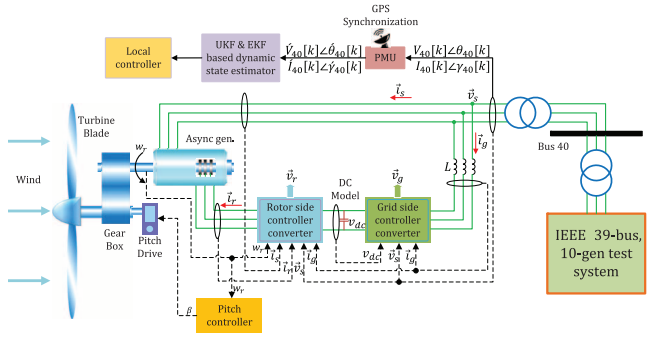

Fig. 1. DFIG connected to the IEEE 39-bus, 10-gen test system with dynamic state estimator.

the dynamics of the rotating machine, i.e., the induction generator, during any interference of the network, which makes PMU voltage and current magnitude and phase angle measurements as inputs/outputs that drive the dynamical equations of the DFIG. This can also facilitate the decentralized implementation of the UKF and EKF algorithms. These estimates of the dynamic states of the DFIG can be utilized to improve the performance of DFIG in power systems, especially for the fault ride through study where DFIG internal sates are involved in the controller design. The dynamic state estimation can realize the acquisition of such internal states, which are otherwise very difficult to obtain.

The rest of the paper is organized as follows. A comprehensive mathematical model for DFIG and its implementation in a complex power system is presented in Section II. UKF and EKF algorithms are presented in Section III. In Section IV, a case study of a DFIG connected to the IEEE 39-bus, 10-generator test system is investigated with bad data detection technique and its implementation in the power system. Finally, a conclusion will be drawn in Section V.

II. Mathematical Model for DFIG

The doubly fed induction generator model can be divided into 5 parts: A) wind turbine (also called drive train), B) asynchronous generator (also called induction generator), C) rotor side controller, D) grid side controller, and E) DC link. Please refer to Fig. 1.

Three reference frames are used in this model: (i) infinity reference d-q frame (or swing bus in real a power system), (ii) stator voltage d-q reference frame, and (iii) mutual flux d-q reference frame, the latter two of which will appear with superscripts, κ and ι respectively. All constants and parameters used in the model are given in the Appendix A.

A. Wind Turbine

The mechanical torque T_m and the mechanical power P_m produced by the wind are related to wind speed V_w and rotor speed w_r as follows [19],

$$T_m = \frac{-P_m}{w_r}, \tag{1}$$

$$P_m = \frac{V_w^3 C_p K P_{m\_nom}}{P_{e\_nom}}, \tag{2}$$

where V_w is wind speed in per unit, P_{m_nom} and P_{e_nom} are the nominal mechanical and electrical power respectively, K is the maximum fraction of mechanical energy that can be extracted from wind energy, and C_p is the mechanical power coefficient, which can be obtained by the following equations,

$$C_p = \frac{c_1(\frac{c_2}{\lambda_r} - c_3\beta - c_4)e^{-c_5/\lambda_r} + c_6\lambda}{C_{p\_nom}}, \tag{3}$$

$$\lambda = \frac{\lambda_{nom}(\frac{w_r}{w_{nom}})}{V_w}, \tag{4}$$

$$\lambda_r = \frac{1}{\frac{1}{\lambda + c_7\beta} - \frac{c_8}{1+\beta^3}}, \tag{5}$$

where C_{p_nom} is the nominal mechanical power coefficient, β is the wind turbine blade pitch angle, λ_{nom} is the nominal tip speed ratio and c_i, $i \in \{1, \ldots, 8\}$ are turbine constants. Sign convention is adopted such that when DFIG is generating power to grid (i.e., generator mode), T_m is negative, whereas when it is consuming power (i.e., motor mode), T_m is positive. In order to keep rotor speed w_r in a reasonable range, a proportional controller for pitch angle is implemented such that the pitch angle β, $0 \le \beta \le 45^o$ and $0 \le \dot{\beta} \le 2^o/s$ can be calculated as,

$$\beta = \begin{cases} k_\beta(w_r - w_D) & \text{if } w_r > w_D \\ 0 & \text{otherwise} \end{cases},$$

where w_D is the maximum angular speed.

B. Asynchronous Generator

Asynchronous generator, also known as induction generator, is analyzed and calculated in mechanical and electrical parts.

1) Mechanical: The relationship between rotor speed w_r, mechanical torque T_m, and electrical torque T_e can be shown by the following differential equation [1],

$$\dot{w}_r = \frac{1}{2H}(T_m - T_e - Fw_r), \tag{6}$$

where electrical torque T_e can be expressed with stator flux (Φ_{ds} and Φ_{qs}) and stator current (i_{ds} and i_{qs}) as

$$T_e = \Phi_{ds} i_{qs} - \Phi_{qs} i_{ds}, \tag{7}$$

where constant H is the generator inertia and F is the friction factor.

2) Electrical: The equivalent circuit of electrical part of asynchronous generator is shown in Fig. 2 with relevant parameters. The following differential equations describe the dynamics of the rotor flux, Φ_{dr} and Φ_{qr} [6],

$$\dot{\Phi}_{dr} = w_b(v_{dr} + (w_s - w_r)\Phi_{qr} - R_r i_{dr}), \tag{8}$$

$$\dot{\Phi}_{qr} = w_b(v_{qr} - (w_s - w_r)\Phi_{dr} - R_r i_{qr}), \tag{9}$$

where $w_b = 2\pi f\ rad/s, f = 60$ Hz is the base angular speed and $w_s = 1$ is the synchronous angular speed in the synchronous frame. Likewise, the dynamics of the stator flux, Φ_{ds} and Φ_{qs}, can be described as follows,

$$\dot{\Phi}_{ds} = w_b(v_{ds} + w_s\Phi_{qs} - R_s i_{ds}), \tag{10}$$

$$\dot{\Phi}_{qs} = w_b(v_{qs} - w_s\Phi_{ds} - R_s i_{qs}). \tag{11}$$

Disregarding the transience of stator flux, the following equations can be obtained,

$$v_{ds} + w_s\Phi_{qs} - R_s i_{ds} = 0, \tag{12}$$
$$v_{qs} - w_s\Phi_{ds} - R_s i_{qs} = 0. \tag{13}$$

Rotor current i_{dr} and i_{qr}, and stator current i_{ds} and i_{qs} can be expressed with additional variables, stator-rotor mutual flux Φ_{dm} and Φ_{qm} as follows,

$$i_{dr} = \frac{\Phi_{dr} - \Phi_{dm}}{L_{lr}}, \tag{14}$$
$$i_{qr} = \frac{\Phi_{qr} - \Phi_{qm}}{L_{lr}}, \tag{15}$$
$$i_{ds} = \frac{\Phi_{ds} - \Phi_{dm}}{L_{ls}}, \tag{16}$$
$$i_{qs} = \frac{\Phi_{qs} - \Phi_{qm}}{L_{ls}}. \tag{17}$$

Stator-rotor mutual flux can be expressed as,

$$\Phi_{dm} = L_{ad}\left(\frac{\Phi_{dr}}{L_{lr}} + \frac{\Phi_{ds}}{L_{ls}}\right), \tag{18}$$
$$\Phi_{qm} = L_{aq}\left(\frac{\Phi_{qr}}{L_{lr}} + \frac{\Phi_{qs}}{L_{ls}}\right), \tag{19}$$

where constants L_{ad} and L_{aq} are the d-q mutual flux factors.

C. Grid Side Controller

Grid Side Control (GSC) scheme, performed in stator voltage reference frame is used to regulate the voltage of DC-link capacitor and the reactive power injected into the GSC.

Stator voltage (i.e., terminal voltage) $v_s\angle\theta$ and grid current $i_g\angle\nu$ can be transformed to stator voltage reference frame with the following equations [20],

$$v_s^\kappa\angle\theta^\kappa = v_s\angle(\theta-\theta) = v_s\angle 0^o, \tag{20}$$
$$i_g^\kappa\angle\nu^\kappa = i_g\angle(\nu-\theta), \tag{21}$$

and d-q components of v_s^κ (v_{ds}^κ and v_{qs}^κ) and i_g^κ (i_{dg}^κ and i_{qg}^κ) are computed accordingly. A PI controller is used to generate $i_{dg\_ref}^\kappa$ according to the following equations,

$$\dot{x}_1 = v_{dc\_nom} - v_{dc}, \tag{22}$$
$$i_{dg\_ref}^\kappa = k_{p1}(v_{dc\_nom} - v_{dc}) + k_{i1}x_1, \tag{23}$$

where x_1 is an intermediate variable. We assign $i_{qg\_ref}^\kappa = 0$ for GSC zero reactive power injection. In the current regulator, the controlled grid side voltage can be calculated using following equations,

$$\dot{x}_2 = i_{dg\_ref}^\kappa - i_{dg}^\kappa, \tag{24}$$
$$\dot{x}_3 = i_{qg\_ref}^\kappa - i_{qg}^\kappa, \tag{25}$$
$$v'_{dg} = k_{p2}(i_{dg\_ref}^\kappa - i_{dg}^\kappa) + k_{i2}x_2, \tag{26}$$
$$v'_{qg} = k_{p2}(i_{qg\_ref}^\kappa - i_{qg}^\kappa) + k_{i2}x_3, \tag{27}$$
$$v_{dg}^\kappa = v_{ds}^\kappa + L_{RL}i_{qg}^\kappa - R_{RL}i_{dg}^\kappa - v'_{dg}, \tag{28}$$
$$v_{qg}^\kappa = v_{qs}^\kappa - L_{RL}i_{dg}^\kappa - R_{RL}i_{qg}^\kappa - v'_{qg}, \tag{29}$$

where x_2, x_3, v'_{dg} and v'_{qg} are intermediate variables. Then grid voltage $v_g\angle\delta$ in infinity synchronous reference frame, shown with $v_g^\kappa\angle\delta^\kappa$ is as follows,

$$v_g = \sqrt{(v_{dg}^\kappa)^2 + (v_{qg}^\kappa)^2}, \quad \delta = \delta^\kappa + \theta. \tag{30}$$

D. Rotor Side Controller

Rotor Side Controller (RSC), performed in mutual flux reference frame is to regulate turbine output active power P_m and the reactive power Q_{elec} which can be measured at the terminal.

The d-q frame components of mutual flux in stator voltage reference frame $\Phi_m^\kappa\angle\alpha^\kappa$ are computed as [7],

$$\Phi_{dm}^\kappa = (i_{ds}^\kappa + i_{dr}^\kappa)L_m, \tag{31}$$
$$\Phi_{qm}^\kappa = (i_{qs}^\kappa + i_{qr}^\kappa)L_m. \tag{32}$$

Rotor current $i_r\angle\mu$ and stator current $i_s\angle\epsilon$ are transformed to mutual flux reference frame as $i_r^\iota\angle\mu^\iota$ and $i_s^\iota\angle\epsilon^\iota$ given below,

$$i_r^\iota\angle\mu^\iota = i_r\angle(\mu - \alpha^\kappa - \theta), \tag{33}$$
$$i_s^\iota\angle\epsilon^\iota = i_s\angle(\epsilon - \alpha^\kappa - \theta). \tag{34}$$

Firstly, a power regulator is utilized to set temporary q-component of the rotor reference current $i_{qr\_ref}^{\star\iota}$, where the input is the difference of reference power P_{ref} and the summation of terminal measured power P_{elec} and power loss P_{loss}, the latter of which includes friction mechanical loss, stator heat loss, rotor heat loss and grid coupling inductor loss. P_{ref}, P_{elec} and P_{loss} are obtained according to the following equations,

$$\begin{aligned} P_{elec} &= -Re[v_s\angle\theta(i_s\angle\epsilon + i_g\angle\mu)^*] \\ &= -[v_{ds}(i_{ds} + i_{dg}) + v_{qs}(i_{qs} + i_{qg})], \end{aligned} \tag{35}$$
$$P_{loss} = w_r^2 F + i_s^2 R_s + i_r^2 R_r + i_g^2 R_{RL}, \tag{36}$$

and

$$P_{ref} = P_{ref}^\star \frac{P_{mech\_nom}}{P_{elec\_nom}}, \tag{37}$$

where

$$P_{ref}^\star = \begin{cases} (w_r - w_A)k_{B\_A} & w_r < w_B \\ (\frac{w_r}{w_C})^3 K & w_B \le w_r < w_C \\ (w_r - w_A)k_{D\_C} + (\frac{w_r}{w_C})^3 K & \text{otherwise} \end{cases}.$$

The current $i_{qr\_ref}^{\star\iota}$ with x_4 being the intermediate variable, is computed by,

$$\dot{x}_4 = P_{ref} - P_{elec} - P_{loss}, \tag{38}$$
$$i_{qr\_ref}^{\star\iota} = k_{p3}(P_{ref} - P_{elec} - P_{loss}) + k_{i3}x_4. \tag{39}$$

Then a reactive power regulator is used to generate temporary d-component of the rotor reference current $i_{dr\_ref}^{\star\iota}$ with the following equations,

$$\dot{x}_5 = Q_{ref} - Q_{elec}, \tag{40}$$
$$i_{dr\_ref}^{\star\iota} = k_{p4}(Q_{ref} - Q_{elec}) + k_{i4}x_5, \tag{41}$$

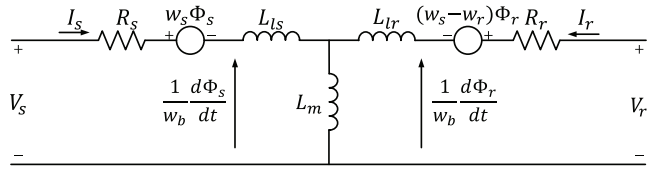

Fig. 2. Equivalent circuit of induction generator.

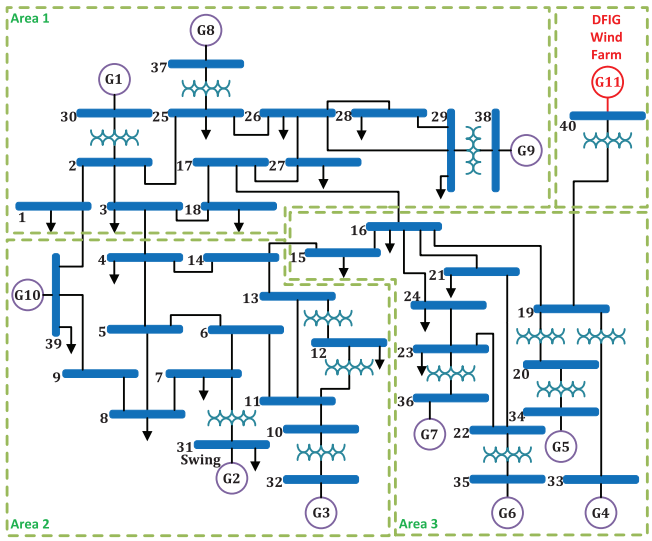

Fig. 3. 40-bus, 11-generator power system.

where x_5 is an intermediate variable and

$$Q_{elec} = -Im[v_s\angle\theta(i_s\angle\epsilon + i_g\angle\mu)^*] \quad (42)$$
$$= -[v_{qs}(i_{ds}+i_{dg}) - v_{ds}(i_{qs}+i_{qg})]. \quad (43)$$

After acquiring the temporary values $i^{\star\iota}_{dr\_ref}$ and $i^{\star\iota}_{qr\_ref}$, rotor reference current $i^{\iota}_{dr\_ref}$ and $i^{\iota}_{qr\_ref}$ are expressed as

$$i^{\iota}_{dr\_ref} = i^{\star\iota}_{dr\_ref}, \quad (44)$$
$$i^{\iota}_{qr\_ref} = \begin{cases} \text{sign}(i^{\star\iota}_{qr\_ref})\sqrt{1-(i^{\star\iota}_{dr\_ref})^2} & i^{\star\iota}_{r\_ref} \geq 1 \\ i^{\star\iota}_{qr\_ref} & i^{\star\iota}_{r\_ref} < 1 \end{cases} \quad (45)$$

where $i^{\star\iota}_{r\_ref} = \sqrt{(i^{\star\iota}_{dr\_ref})^2 + (i^{\star\iota}_{qr\_ref})^2}$. Rotor side current regulator, similar to stator side is also used to generate controlled rotor voltage v^{ι}_{dr} and v^{ι}_{qr}, which are computed as follows,

$$\dot{x}_6 = i^{\iota}_{dr\_ref} - i^{\iota}_{dr}, \quad (46)$$
$$\dot{x}_7 = i^{\iota}_{qr\_ref} - i^{\iota}_{qr}, \quad (47)$$
$$v'_{dr} = k_{p5}(i^{\iota}_{dr\_ref} - i^{\iota}_{dr}) + k_{i5}x_6, \quad (48)$$
$$v'_{qr} = k_{p5}(i^{\iota}_{qr\_ref} - i^{\iota}_{qr}) + k_{i5}x_7, \quad (49)$$
$$v^{\iota}_{dr} = R_r i^{\iota}_{dr} - (w_s - w_r)[L_r i^{\iota}_{qr} + L_m i^{\iota}_{qs}] + v'_{dr}, \quad (50)$$
$$v^{\iota}_{qr} = R_r i^{\iota}_{qr} + (w_s - w_r)[L_r i^{\iota}_{dr} + L_m i^{\iota}_{ds}] + v'_{qr}, \quad (51)$$

where x_6, x_7, v'_{dr} and v'_{qr} are intermediate variables and constant $L_r = L_{lr} + L_m$. Rotor voltage $v_r\angle\eta$, in infinity synchronous frame is expressed with $v^{\iota}_r\angle\eta^{\iota}$ as follows,

$$v_r\angle\eta = \sqrt{(v^{\iota}_{dr})^2 + (v^{\iota}_{qr})^2}\angle\eta^{\iota} + \alpha^{\kappa} + \theta. \quad (52)$$

E. DC Link

After obtaining grid voltage $v_g\angle\delta$ and rotor voltage $v_r\angle\eta$, i.e., $v_{dg}, v_{qg}, v_{dr}, v_{qr}$, grid side current can easily be acquired by [4]

$$i_{dg} = \frac{v_{ds} - v_{dg}}{R_{RL}}, \quad (53)$$
$$i_{qg} = \frac{-(v_{qs} - v_{qg})}{L_{RL}}. \quad (54)$$

Grid side power and rotor side power P_g and P_r can be calculated by

$$P_g = -(v_{dg}i_{dg} + v_{qg}i_{qg}), \quad (55)$$
$$P_r = -(v_{dr}i_{dr} + v_{qr}i_{qr}). \quad (56)$$

With energy conservation equation, the power stored in the DC-link capacitor P_{dc} can be written as,

$$P_{dc} = P_r - P_g = C_{dc}v_{dc}\dot{v}_{dc}, \quad (57)$$

hence the following differential equation holds,

$$\dot{v}_{dc} = \frac{P_r - P_g}{C_{dc}v_{dc}}. \quad (58)$$

Differential (6), (8), (9), (58), (22), (24), (25), (38), (40), (46), (47) together with algebraic (12), (13), (14), (15), (16), (17), (53) and (54) form the set of 19 dynamic and algebraic equations for the doubly fed induction generator with dynamic state variable vector $[w_r, \phi_{dr}, \phi_{qr}, x_1, x_2, x_3, v_{dc}, x_4, x_5, x_6, x_7]^T$, algebraic variable vector $[\phi_{ds}, \phi_{qs}, i_{dr}, i_{qr}, i_{ds}, i_{qs}, i_{dg}, i_{qg}]^T$, pseudo-input vector $[V_{40}, \theta_{40}]^T$, and output vector $[I_{40}, \gamma_{40}]^T$.

Here we consider a modification to IEEE 39-bus, 10-generator test system with DFIG wind farm connected to bus 40, which is then connected to bus 19 through a transformer. The modified power system shown in Fig. 3 is now comprised of 40 buses and 11 generators.

The dynamic behavior of DFIG, which is connected to an IEEE 39-bus, 10-generator test system, can be expressed in the following compact form,

$$\dot{\tilde{x}}_{11} = \tilde{f}_{11}(\tilde{x}_{11}, \tilde{z}_{11}, \tilde{u}_{11}), \quad (59)$$
$$0 = \tilde{g}_{11}(\tilde{x}_{11}, \tilde{z}_{11}, \tilde{u}_{11}), \quad (60)$$
$$\tilde{y}_{11} = \tilde{h}_{11}(\tilde{x}_{11}, \tilde{z}_{11}, \tilde{u}_{11}), \quad (61)$$

where $\tilde{x}_{11}$ is the DFIG dynamic state variable vector, $\tilde{z}_{11}$ consists of the DFIG algebraic variables, $\tilde{u}_{11}$ is the DFIG pseudo-input vector and $\tilde{y}_{11}$ represents the total current flowing into bus 40. Both the pseudo-input and output of the DFIG are measured using PMUs, placed at bus 40, see Fig. 1. Similarly, the dynamic equations for the rest generators G1 to G10 can also be expressed in the same compact form, so all the 11 generators can be described as,

$$\dot{\tilde{x}}_i = \tilde{f}_i(\tilde{x}_i, \tilde{z}_i, \tilde{u}_i), \quad (62)$$
$$0 = \tilde{g}_i(\tilde{x}_i, \tilde{z}_i, \tilde{u}_i), \quad (63)$$
$$\tilde{y}_i = \tilde{h}_i(\tilde{x}_i, \tilde{z}_i, \tilde{u}_i), \quad (64)$$

for $i \in \{1, \ldots, 11\}$, where state vector $\tilde{x}_i$ consists of dynamic states of each generator, $\tilde{z}_i$ is the algebraic variable vector of

each generator, $\tilde{u}_i$ is the pseudo-input vector comprised of terminal voltage and phase angle $V_i\angle\theta_i$ of all generator buses and $\tilde{y}_i$, the output vector represents the total current $I_i\angle\gamma_i$ flowing into each respective generator bus bar and $\tilde{f}_i$, $\tilde{g}_i$ and $\tilde{h}_i$ are known functions. For equations describing the dynamics of 10 generators in the IEEE 39 bus, 10-generator test system, see [11]. Substituting $\tilde{z}_i$ from (63) into (62) and (64), the previous compact form can be rewritten as,

$$\dot{\tilde{x}}_i = \tilde{f}_i(\tilde{x}_i, \tilde{u}_i), \tag{65}$$

$$\tilde{y}_i = \tilde{h}_i(\tilde{x}_i, \tilde{u}_i), \tag{66}$$

for $i \in \{1, \ldots, 11\}$. The initial condition of this dynamical system can be acquired with (65) and (66). Assuming the system is initially operating at steady state, (65) and (66) become

$$0 = \tilde{f}_i(\tilde{x}_i, \tilde{u}_i), \tag{67}$$

$$\tilde{y}_i = \tilde{h}_i(\tilde{x}_i, \tilde{u}_i). \tag{68}$$

Solving (67) and (68) will issue the initial condition of the dynamical system for the simulation. Equations (65) and (66) together with the following power balance equation describe the whole power system [21],

$$P_{Ll}(t) + jQ_{Ll}(t) + v_l(t)e^{j\theta_l(t)}i_l(t)e^{-j\gamma_l(t)} - \sum_{r=1}^{40} v_l(t)v_r(t)Y_{lr}e^{j(\theta_l(t)-\theta_r(t)-\phi_{lr})} = 0, \tag{69}$$

where $Y_{lr}\angle\phi_{lr}$ is the admittance of the line connecting bus l and r, $P_{Ll}(t)$ and $Q_{Ll}(t)$ are active power and reactive power consumed by the loads connected to busbar l at time t. As only the dynamic states of DFIG are to be estimated, i.e., $i = 11$, we notate $\tilde{x}_{11}$ as x, $\tilde{y}_{11}$ as y, $\tilde{u}_{11}$ as u, $\tilde{f}_{11}$ as f, $\tilde{h}_{11}$ as h, $V_{40}\angle\theta_{40}$ as $V\angle\theta$ and $I_{40}\angle\gamma_{40}$ as $I\angle\gamma$. So the discretized system with noisy PMU measurements can be expressed by

$$\begin{aligned} x[k] &= f(x[k-1], V[k-1], \acute{\theta}[k-1], \xi[k-1], \mathcal{C}), \\ \acute{y}[k] &= h(x[k], \acute{V}[k], \acute{\theta}[k], \xi[k], \mathcal{C}) + \zeta[k], \end{aligned} \tag{70}$$

where diacritic sign $\acute{(\cdot)}$ denotes a measurement of $(\cdot)$ affected by noise and $\mathcal{C} = [v_{dr}, v_{qr}, v_{ds}, v_{qs}]$ is the controlled variable vector of GSC and RSC. Voltage and current measurement noise $\xi^{2\times1}$ and $\zeta^{2\times1}$ respectively, are distributed normally with zero mean and covariance Q and R as follows,

$$\xi[k] \sim \mathcal{N}([0]_{2\times1}, Q), \tag{71}$$

$$\zeta[k] \sim \mathcal{N}([0]_{2\times1}, R), \tag{72}$$

and

$$Q = \begin{bmatrix} \sigma_{\xi_1}^2 & 0 \\ 0 & \sigma_{\xi_2}^2 \end{bmatrix}, R = \begin{bmatrix} \sigma_{\zeta_1}^2 & 0 \\ 0 & \sigma_{\zeta_2}^2 \end{bmatrix}. \tag{73}$$

In the DFIG dynamical system, the voltage is considered as the input and the current is the output. In the dynamic state estimator, however, voltage and current both are inputs and the estimated states are the outputs. The DFIG dynamical equations are formulated in this manner so that the output of the system, the current, can be acquired by both PMU direct measurement and through the calculation by estimated states. The error in the predicted output and measured output is the innovation process that drives the estimator.

III. Estimation Algorithms

A. Unscented Kalman Filter

The unscented transformation (UT) is a method to estimate statistics of a random variable subjected to a given nonlinear transformation [13]. Let us assume that υ is a τ dimensional random variable distributed normally with mean $\bar{\upsilon}$ and covariance $P_{\upsilon\upsilon}$. If υ undergoes a nonlinear transformation $\psi = \Upsilon(\upsilon)$, then UT can provide the estimation of the mean $\bar{\psi}$ and covariance $P_{\psi\psi}$ of ψ. A set of $2\tau + 1$ points called sigma points (χ) with mean $\bar{\upsilon}$ and covariance $P_{\upsilon\upsilon}$ are chosen to estimate the mean $(\bar{\psi})$ and covariance $(P_{\psi\psi})$ of the transformed points using the following equations [22],

$$\begin{aligned} \chi^0 &= \bar{\upsilon}, \\ \chi^r &= \bar{\upsilon} + \left(\sqrt{(\tau+\lambda)P_{\upsilon\upsilon}}\right)^r; r \in \{1, 2, \ldots, \tau\}, \\ \chi^{r+\tau} &= \bar{\upsilon} - \left(\sqrt{(\tau+\lambda)P_{\upsilon\upsilon}}\right)^r; r \in \{1, 2, \ldots, \tau, \}, \end{aligned} \tag{74}$$

where $\left(\sqrt{(\tau+\lambda)P_{\upsilon\upsilon}}\right)^r$ is the rth row or column of the matrix square root of $(\tau+\lambda)P_{\upsilon\upsilon}$. Also $\lambda = a^2(\tau+\kappa) - \tau$ is a scaling parameter where a is a factor which specifies the spread of the sigma points, and $\kappa = 0$ is the second scaling parameter. Furthermore, mean and covariance of ψ are approximated based on the following corresponding weights,

$$W_m^0 = \frac{\lambda}{(\lambda+\tau)}, W_c^0 = \frac{\lambda}{(\lambda+\tau)} + (1 - a^2 + b), \tag{75}$$

$$W_m^r = W_c^r = \frac{1}{2(\lambda+\tau)}; \quad r \in \{1, 2, \ldots, 2\tau\}, \tag{76}$$

where b is a factor to incorporate prior knowledge of the distribution of υ, e.g., $b = 2$ for normal distributions. The mean and covariance of the random variable ψ can be calculated using the following equations,

$$\psi^r = \Upsilon(\chi^r), \quad r \in \{0, 1, \ldots, 2\tau\}, \tag{77}$$

$$\bar{\psi} = \sum_{r=0}^{2\tau} W_m^r \psi^r, \tag{78}$$

$$P_{\psi\psi} = \sum_{r=0}^{2\tau} W_c^r (\psi^r - \bar{\psi})(\psi^r - \bar{\psi})^T. \tag{79}$$

Now consider the decoupled dynamic of the k^{th} iteration (70). As discussed before, PMU measurement noise is assumed to have a normal distribution with zero mean. If we assume the covariances of measurement noise in pseudo inputs are constant then the state vector $x[k]$ and measurement noise $\xi[k]$ can be considered as a new augmented state vector, $X[k] = [x[k]\xi[k]]^T$, where $X[k] \in \mathbb{R}^{(n+2)\times1}$ is the augmented state vector. Predicted augmented state vector $\hat{X}[k]$ and its covariance can be obtained as follows,

$$\hat{X}[k] = \begin{bmatrix} \hat{x}[k] & [0]_{2\times1} \end{bmatrix}^T, \tag{80}$$

$$\hat{P}_{XX}[k] = \begin{bmatrix} P_{xx}[k] & P_{x\xi}[k] \\ P_{x\xi}[k] & Q \end{bmatrix}. \tag{81}$$

Using the unscented transformation, state estimation of DFIG can be implemented using the following filtering algorithm,

Step 0:
- Set $\xi = 0$ and let $a = 10^{-3}$, $b = 2$.
- Select initial value of the state vector $x[0]$ and select it as $\bar{x}[0]$.
- Augment initial value of the state vector with PMU measurement noise mean, i.e., $\hat{X}[0] = [\,\hat{x}[0] \quad [0]_{2\times 1}\,]^T$.
- Initiate covariance of the augmented state vector $X[0]$ as $\hat{P}_{XX}[0] = \begin{bmatrix} P_{xx}[0] & 0 \\ 0 & Q \end{bmatrix}$.
- Set $k = 1$.

Step 1: Time Update,
- Consider $\bar{v} = X[k-1]$ and $P_{vv} = \hat{P}_{XX}[k-1]$ in (74).
- Generate $2(n+2)+1$ sigma points according to (74), i.e., $\chi[k-1] = [\,\chi^0[k-1] \quad \cdots \quad \chi^{2(n+2)}[k-1]\,]$.
- Associate weights according to (75) and (76), i.e.,

$$W_m = \begin{bmatrix} W_m^0 & W_m^1 & \cdots & W_m^{2(n+2)} \end{bmatrix},$$
$$W_c = \begin{bmatrix} W_c^0 & W_c^1 & \cdots & W_c^{2(n+2)} \end{bmatrix}.$$

- Calculate transferred points according to (77), i.e., $\tilde{X}^r[k] = f(\chi^r[k-1], \acute{u}[k-1], \mathcal{C})$.
- Calculate mean $\bar{X}[k]$ and covariance $P_{\tilde{X}\tilde{X}}$ of the transferred points $\tilde{X}[k]$, according to (78) and (79) with ψ replaced by $\tilde{X}$ and $\bar{\psi}$ replaced by $\bar{X}$.

Step 2: Measurement Update,
- Calculate measurement update based on the transferred sigma points $\tilde{X}[k]$ obtained from Step 1, i.e., $\tilde{Y}[k] = h(\tilde{X}[k], \acute{u}[k])$.
- Calculate mean $\bar{Y}[k]$ according to (78) with $\psi = \tilde{Y}$
- Calculate covariance of $\tilde{Y}[k]$, $P_{\tilde{Y}\tilde{Y}}$, according to (79), i.e.,

$$P_{\tilde{Y}\tilde{Y}} = R + \sum_{r=0}^{2(n+2)} W_c^r \left(\tilde{Y}^r[k] - \bar{Y}[k]\right)\left(\tilde{Y}^r[k] - \bar{Y}[k]\right)^T.$$

- Calculate cross-covariance $P_{\tilde{X}\tilde{Y}}$ as,

$$P_{\tilde{X}\tilde{Y}} = \sum_{r=0}^{2(n+2)} W_c^r \left(\tilde{X}^r[k] - \bar{X}[k]\right)\left(\tilde{Y}^r[k] - \bar{Y}[k]\right)^T.$$

Step 3: Filtering,
- Calculate filter gain $\mathcal{K}[k]$ as, $\mathcal{K}[k] = P_{\tilde{X}\tilde{Y}} P_{\tilde{Y}\tilde{Y}}^{-1}$.
- Update predicted states based on PMU measurement as, $\hat{X}[k] = \bar{X}[k] + \mathcal{K}[k](\acute{y}[k] - \bar{Y}[k])$.
- Calculate covariance $\hat{P}_{XX}[k]$ as, $\hat{P}_{XX}[k] = P_{\tilde{X}\tilde{X}} - \mathcal{K}[k] P_{\tilde{Y}\tilde{Y}} \mathcal{K}^T[k]$.

Step 4:
- Reset $\hat{P}_{XX}[k]$ to $\begin{bmatrix} P_{xx}[k] & P_{x\xi}[k] \\ P_{x\xi}[k] & Q \end{bmatrix}$.
- Reset $\hat{X}[k]$ to $[\,\hat{x}[k] \quad [0]_{2\times 1}\,]^T$.
- Increment k and goto Step 1.

At the end of each filtering algorithm iteration $\hat{X}[k]$ provides on-line estimate of generator augmented state vector $X[k]$. Estimation of the state vector $x[k]$ can be extracted from the augmented state vector $\hat{X}[k]$ according to (80).

B. Extended Kalman Filter

Introducing covariance matrix $Q_d^{(n+2)\times(n+2)}$,

$$Q_d = \begin{bmatrix} 0 & \cdots & 0 & 0 \\ \vdots & \ddots & \vdots & \vdots \\ 0 & \cdots & \sigma_{\xi_1}^2 & 0 \\ 0 & \cdots & 0 & \sigma_{\xi_2}^2 \end{bmatrix}. \tag{82}$$

EKF algorithm is explained in brief as follows,

Step 0: Initialization. See UKF algorithm Step 0.
Step 1:
- Predicted state estimation $\tilde{X}[k] = f(\hat{X}[k-1], \acute{u}[k-1], \mathcal{C})$,
- Predicted covariance estimation $P^-[k] = F[k-1]\hat{P}[k-1]F[k-1]^T + Q_d$, where Jacobian Matrix $F[k-1]$ is

$$F[k-1] = \left.\frac{\partial f}{\partial X}\right|_{\hat{X}[k-1], \acute{u}[k-1], \mathcal{C}}. \tag{83}$$

Step 2:
- Innovation Covariance $S[k] = H[k]P^-[k]H[k]^T$,
- Kalman gain $\mathcal{K}[k] = P^-[k]H[k]^T S[k]^{-1}$, where Jacobian Matrix $H[k]$ is computed as follows,

$$H[k] = \left.\frac{\partial h}{\partial X}\right|_{\tilde{X}[k], \acute{u}[k], \mathcal{C}}. \tag{84}$$

Step 3:
- Update state estimation $\hat{X}[k] = \tilde{X}[k] + \mathcal{K}[k][\acute{y}[k] - h(\tilde{X}[k], \acute{u}[k], \mathcal{C})]$,
- Update covariance estimation $\hat{P}[k] = (I - \mathcal{K}[k]H[k])P^-[k]$.

Step 4: Reset $\hat{P}[k]$ and $\hat{X}[k]$ and perform next iteration.

IV. Numerical Results

A. Case Study

The 40-bus, 11-generator test system considered in this paper consists of one DFIG wind farm and 10 synchronous generators. These 10 synchronous generators are in three separate areas, and in each area one generator has a type I, IEEE ST1A AVR with PSS excitation system and all other generators are equipped with excitation systems of type II, IEEE DC1A AVR without PSS. Speed-governing systems of the 10 generators are categorized into two main types: (i) mechanical-hydraulic and (ii) electro-hydraulic with/without steam feedback. Hydro and steam turbines are also considered in the generation units. All the implemented steam turbines are tandem-compound, double or single reheat type. For generator and speed-governing equations, see [11] and [23]. The simulation is conducted in time domain and PMU measured values $V\angle\theta$ and $I\angle\gamma$ are sampled at 100 Hz. As shown in Fig. 1, PMUs measure the magnitudes and phase angles of voltage and current of bus 40. $V_{40}\angle\theta_{40}$ and $I_{40}\angle\gamma_{40}$ are the RMS phase voltage and current in per unit system at bus 40. The measured voltage and current are assumed to have white noises in both magnitudes and phase angles. Thus, $\acute{V}_{40}\angle\acute{\theta}_{40}$ and $\acute{I}_{40}\angle\acute{\gamma}_{40}$ are the noisy PMU measurements of voltage and current of bus 40. The dynamical system

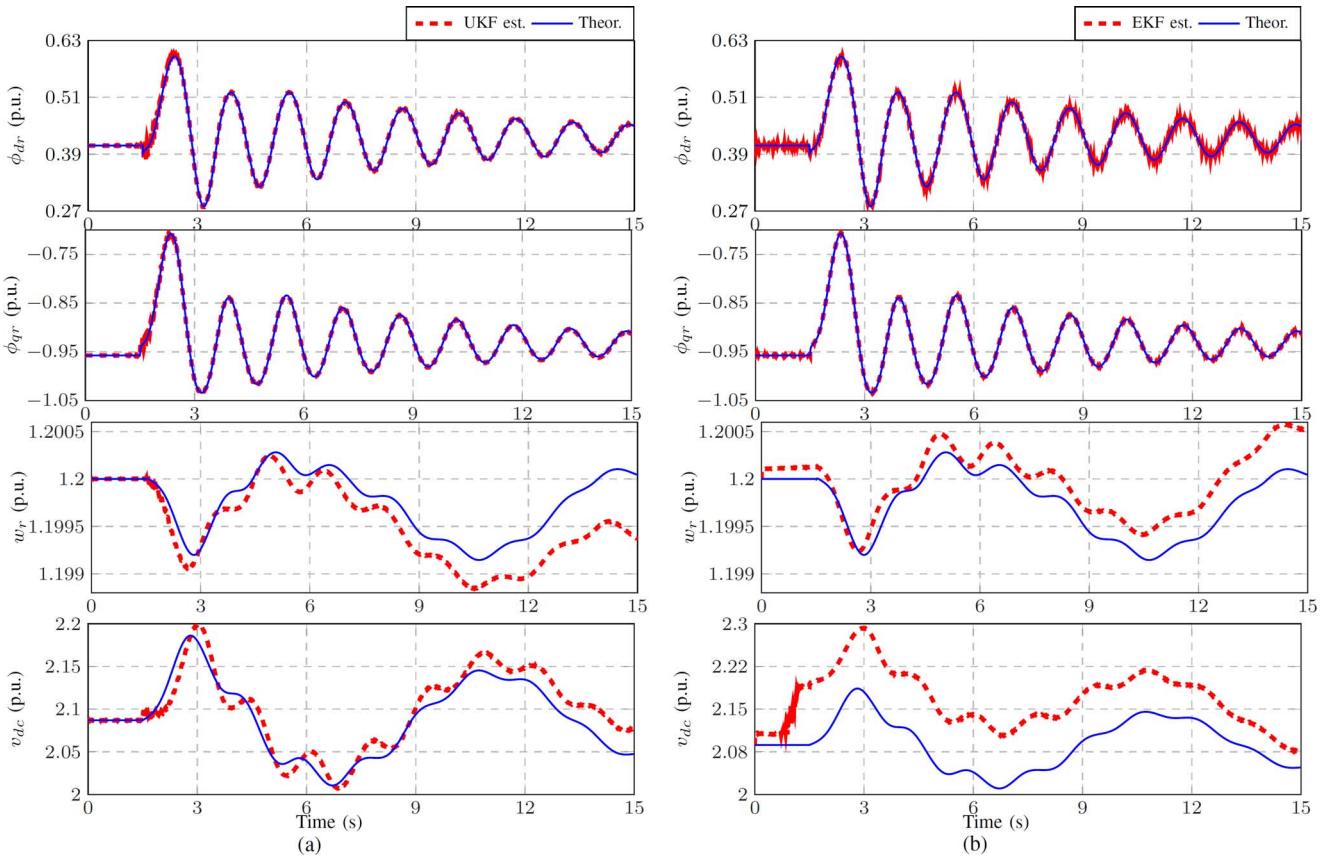

Fig. 4. Dynamic state estimation for case study.

described in the form (65) and (66) consists of measurable inputs and outputs-voltage and current. There are no unknown inputs or unknown outputs in the dynamical equations. The measurements are corrupted by white noises, which is the reason for using UKF and EKF to obtain the state estimates.

The power system operates for 15 seconds with a constant wind speed. During the first 1.5 seconds, the whole power system works at steady state and a flat curve is expected. At 1.5 second, an electric fault occurs and the transmission line between bus 23 and bus 24 is disconnected which remains untouched throughout the rest of simulation. Both UKF and EKF continuously estimate the dynamic states of the DFIG. Fig. 4 presents a comparison of the estimated states from UKF and EKF. It is easy to see that EKF displays a relatively poorer performance than UKF. For state estimation of ϕ_{dr} and ϕ_{qr}, UKF and EKF produce a pair of comparable result but EKF curve contains more fluctuations, which indicates that EKF method is more susceptible to noises than UKF. As for the estimation of w_r, though it does not change noticeably in magnitude during the whole process (actually stays at 1.20), the curve has fast but tiny changes over time. The result of both methods, however, are within the acceptable range, and the discrepancies of them to theoretical result fall in the range of $10^{-5} \sim 10^{-4}$. The superiority of UKF becomes more evident in the estimation of the most nonlinear state v_{dc}. The EKF estimate of v_{dc} error is nearly unacceptable as can be seen in Fig. 4.

EKF is mostly used to deal with quasi-linear systems by simply linearizing the state space and substituting the linearized functions back to linear filters [24]. In other words, EKF propagates the mean and covariance in a linear behavior, which leads to inevitable inaccuracy in state estimation in highly nonlinear state space equations. But UKF makes use of unscented transformation, a deterministic sampling technique to pick a minimum set of sigma points around the mean [25], which explains why the nonlinear behavior of the DFIG is better captured by the UKF algorithm.

B. Bad Data Detection

PMU measurements may, in additional to noises, also have gross errors that deviate significantly from the real data. These measurements, if used, will generate unacceptable discrepancies to estimated data. Therefore, bad data must be detected and eliminated from PMU measurement pool. Before performing this technique, the concept of normalized innovation ratio [10] is introduced as follows,

$$\varrho_{y,1} = \frac{\acute{y}_1[k] - \bar{Y}_1[k]}{\sqrt{P_{\tilde{Y}\tilde{Y}(1,1)}[k]}} \text{ and } \varrho_{y,2} = \frac{\acute{y}_2[k] - \bar{Y}_2[k]}{\sqrt{P_{\tilde{Y}\tilde{Y}(2,2)}[k]}} \tag{85}$$

$\varrho_{y,1}$ and $\varrho_{y,2}$ indicate the deviation ratios of predicted measurements to actual PMU output measurement. When the absolute value of ratios exceed certain thresholds $\varrho_{th,1}$ and $\varrho_{th,2}$ respectively, bad data occur. And the source of bad data can be either

or both of pseudo-input vector $[V, \theta]^T$ and output measurement vector $[I, \gamma]^T$. The modified UKF algorithm with bad data detection methodology is shown as follows,

---

Step 1: Perform first two steps of UKF algorithm.
Step 2: Acquire normalized innovation ratios according to (85).
Step 3:

- (1) If $\varrho_{y,1} < \varrho_{th,1}$ and $\varrho_{y,2} < \varrho_{th,2}$, go to Step 4.
- (2) If $\varrho_{y,1} > \varrho_{th,1}$ and $\varrho_{y,2} < \varrho_{th,2}$, $\acute{y}_1[k] = \bar{Y}_1[k]$ and go to Step 4.
- (3) If $\varrho_{y,1} < \varrho_{th,1}$ and $\varrho_{y,2} > \varrho_{th,2}$, $\acute{y}_2[k] = \bar{Y}_2[k]$ and go to Step 4.
- (4) If $\varrho_{y,1} > \varrho_{th,1}$ and $\varrho_{y,2} > \varrho_{th,2}$, store current vector $u[k]$ and use the latest uncorrupted input vector $u[k-1]$ to acquire a new set of $\varrho_{y,1}$ and $\varrho_{y,2}$.
- (5) If $\varrho_{y,1} < \varrho_{th,1}$ and $\varrho_{y,2} < \varrho_{th,2}$, discard stored $u[k]$ and replaced it with $u[k-1]$. Go to Step 4.
- (6) If $\varrho_{y,1} > \varrho_{th,1}$ and $\varrho_{y,2} < \varrho_{th,2}$, $\acute{y}_1[k] = \bar{Y}_1[k]$, discard stored $u[k]$ and replace it with $u[k-1]$. Go to Step 4.
- (7) If $\varrho_{y,1} < \varrho_{th,1}$ and $\varrho_{y,2} > \varrho_{th,2}$, $\acute{y}_2[k] = \bar{Y}_2[k]$, discard stored $u[k]$ and replace it with $u[k-1]$. Go to Step 4.
- (8) If $\varrho_{y,1} > \varrho_{th,1}$ and $\varrho_{y,2} > \varrho_{th,2}$, then $\acute{y}_1[k] = \bar{Y}_1[k]$ and $\acute{y}_2[k] = \bar{Y}_2[k]$, continue to the next step.
- (9) Use stored $u[k]$ to acquire a new set of $\varrho_{y,1}$ and $\varrho_{y,2}$ with the output obtained in Step 3.8.
- (10) If $\varrho_{y,1} < \varrho_{th,1}$ and $\varrho_{y,2} < \varrho_{th,2}$, keep $u[k]$ and go to Step 4.
- (11) If $\varrho_{y,1} > \varrho_{th,1}$ and $\varrho_{y,2} > \varrho_{th,2}$, abandon $u[k]$ and replace it with $u[k-1]$. Go to Step 4.

Step 4: Perform last two steps of UKF algorithm.

Bad data can exist in pseudo-input vector or/and output vector. Faulty data in either or both of pseudo-input elements will affect $\varrho_{y,1}$ and $\varrho_{y,2}$ significantly, whereas bad data present in output measurement only affects its corresponding normalized innovation ratio, i.e., corrupted $\acute{y}_1[k]$ only affects $\varrho_{y,1}$. If there are no bad data, the detection scheme will stop at Step 3.1 and continue to Step 4. If bad data are in either of the output measurement elements (I, γ), it is to be detected in Step 3.2 or Step 3.3, and then faulty output measurement is discarded and replaced with the predicted output. If bad data are in either or both of pseudo-input items (V, θ) and output measurement is robust, then Step 3.4 will be triggered and detection stops and returns at Step 3.5. This means $u[k]$ is corrupted and so $u[k-1]$ replaces it, and continue onto the next iteration. If bad data exist in (i) both pseudo-input and output measurement vectors with one or two elements in both of them infected or (ii) both of output measurement elements are corrupted with reliable pseudo-input vector, Step 3.4 will be triggered but the provenance of faulty data are unclear. At Step 3.4, we tentatively postulate there are bad data in pseudo-input vector, so current pseudo-input vector $u[k]$ is stored and $u[k-1]$ is used to generate a new, reliable predicted output vector. Step 3.6 or Step 3.7, if activated, indicates that bad data exist in pseudo-input and one of the measured output elements. Therefore, this pseudo-input vector sample is abandoned and replaced by $u[k-1]$ and faulty measured output element is eliminated and renewed with predicted output. If Step 3.8 is true, it can be inferred that bad data exist in both items of output measurement but the accuracy of pseudo-input is unknown. Proceed to next step to make further judgment. If Step 3.10 is satisfied there is no bad data in pseudo-input vector and $u[k]$ is preserved for the next iteration. Lastly, if Step 3.11 is triggered, it indicates the presence of bad data dwells in current pseudo-input sample and hence, $u[k]$ is ditched and $u[k-1]$ takes its place. It should be noted that there is no necessity to tell which one of pseudo-input elements is corrupted as when either or both of them are faulty, the predicted output is highly erroneous and thus the whole vector is discarded.

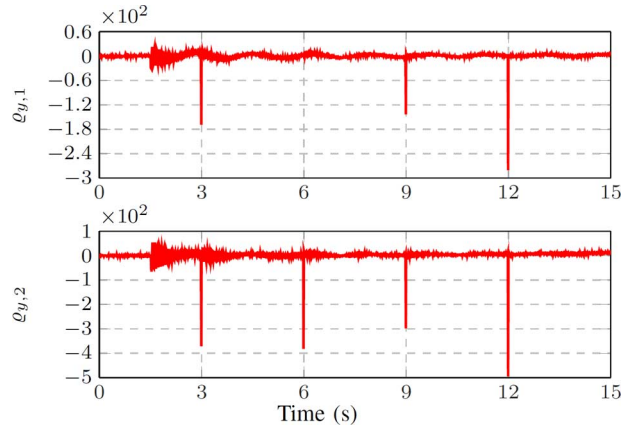

Fig. 5. $\varrho_{y,1}$, $\varrho_{y,2}$ with bad data.

At $t = 3$ s, a bad datum is added to one of pseudo-input element V and no faulty data appear in output measurement. From Fig. 5 it is clear that $\varrho_{y,1}$ and $\varrho_{y,2}$ shoot out significantly above the threshold and Step 3.4 and Step 3.5 are activated. At $t = 6$ s, a bad datum is forged in output measurement item γ and pseudo-input vector is trustworthy. It can be seen that $\varrho_{y,2}$ becomes boundless and only Step 3.3 is triggered. At $t = 9$ s, bad data are made existent in both items of output measurement I and γ. It is evident in the figure that both normalized innovation ratios are abnormal and Step 3.4, Step 3.8, Step 3.9 and Step 3.10 are invoked as expected. Finally, at $t = 12$ s, all elements in both pseudo-input and output measurement vectors are adulterated with bad data. Fig. 5 shows the phenomenal abnormality in both $\varrho_{y,1}$ and $\varrho_{y,2}$ bad data create. In the bad data detection scheme, Step 3.4, Step 3.8, Step 3.9 and Step 3.11 are triggered. With bad data detection and elimination incorporated in UKF algorithm, the simulation result for case 1 with bad data is identical to the result obtained without bad data.

TABLE I
DFIG CONSTANTS AND PARAMETERS

Wind Turbine			
$H = 5.04$pu	$F = 0.11$pu/pu	$w_{nom} = 1.2$	$V_{w_nom} = 12$m/s
$\lambda_{nom} = 8.1$	$K = 0.73$	$k_\beta = 500$	$P_{e_nom} = 1.5e^6/0.9$W
$c_1 = 0.5176$	$c_2 = 116$	$c_3 = 0.4$	$P_{m_nom} = 1.5e^6$W
$c_4 = 0.5$	$c_5 = 21$	$c_6 = 0.0068$	$C_{p_nom} = 0.48$pu
$c_8 = 0.035$	$c_7 = 0.08$		
GSC			
$k_{p1} = 0.002$	$k_{i1} = 0.05$	$L_{RL} = 0.15$pu	$R_{RL} = 0.0015$pu
$k_{p2} = 1$	$k_{i2} = 100$	$C_{dc} = 0.05$pu	$v_{dc_nom} = 2.087$pu
RSC			
$k_{p3} = 1$	$k_{i3} = 100$	$k_{p4} = 0.05$	$k_{i4} = 5$
$k_{p5} = 0.3$	$k_{i5} = 8$	$w_A = 0.7$pu	$w_B = 0.71$pu
$w_C = 1.2$pu	$w_D = 1.21$pu	$k_{BA} = 15.12$	$k_{DC} = 27$

V. CONCLUSION

In this paper, we have presented a general framework for the doubly fed induction generator in order to facilitate the dynamic estimation of the states of DFIG. The proposed method is decentralized and performed with UKF and EKF algorithms using noisy PMU measurements. Comparison of UKF and EKF estimates shows that UKF can provide a better dynamic state estimation of DFIG. The estimation is based on a holistic level where the whole network topology is considered. Bad data detection technique is investigated in depth and it enhances the capacity of error tolerance and self-correction of power systems. The success of the theoretical understanding and simulation of estimating unmeasurable states in a power system lays us a solid foundation on which control scheme may be designed to reinforce the stability of a DFIG power system.

APPENDIX

Table I lists the DFIG constants and parameters.

REFERENCES

[1] A. Feijóo, J. Cidrás, and C. Carrillo, "A third order model for the doubly-fed induction machine," *Electr. Power Syst. Res.*, vol. 56, no. 2, p. 121, 2000.

[2] Y. Mishra, S. Mishra, F. Li, Z. Y. Dong, and R. C. Bansal, "Small-signal stability analysis of a DFIG-based wind power system under different modes of operation," *IEEE Trans. Energy Convers.*, vol. 24, no. 4, pp. 972–982, Dec. 2009.

[3] F. Wu, X.-P. Zhang, K. Godfrey, and P. Ju, "Small signal stability analysis and optimal control of a wind turbine with doubly fed induction generator," *IET Gener., Transm., Distrib.*, vol. 1, no. 5, pp. 751–760, 2007.

[4] F. Wu, X.-P. Zhang, P. Ju, and M. J. Sterling, "Decentralized nonlinear control of wind turbine with doubly fed induction generator," *IEEE Trans. Power Syst.*, vol. 23, no. 2, pp. 613–621, May 2008.

[5] R. Pena, J. Clare, and G. Asher, "Doubly fed induction generator using back-to-back PWM converters and its application to variable-speed wind-energy generation," *IEE Proc.-Electr. Power Applicat.*, vol. 143, no. 3, pp. 231–241, 1996.

[6] L. Yang, Z. Xu, J. Østergaard, Z. Y. Dong, K. P. Wong, and X. Ma, "Oscillatory stability and eigenvalue sensitivity analysis of a DFIG wind turbine system," *IEEE Trans. Energy Convers.*, vol. 26, no. 1, pp. 328–339, Mar. 2011.

[7] L. Yang, Z. Xu, J. Østergaard, Z. Y. Dong, and K. P. Wong, "Advanced control strategy of DFIG wind turbines for power system fault ride through," *IEEE Trans. Power Syst.*, vol. 27, no. 2, pp. 713–722, May 2012.

[8] M. Mokhtari and F. Aminifar, "Toward wide-area oscillation control through doubly-fed induction generator wind farms," *IEEE Trans. Power Syst.*, vol. 29, no. 6, pp. 2985–2992, Nov. 2014.

[9] M. Derafshian and N. Amjady, "Optimal design of power system Stabilizer for power systems including doubly fed induction generator wind turbines," *Energy*, vol. 84, pp. 1–14, 2015.

[10] A. K. Singh and B. C. Pal, "Decentralized dynamic state estimation in power systems using unscented transformation," *IEEE Trans. Power Syst.*, vol. 29, no. 2, pp. 794–804, Mar. 2014.

[11] K. Emami, T. H. Fernando, H. H.-C. Iu, H. Trinh, and K. P. Wong, "Particle filter approach to dynamic state estimation of generators in power systems," *IEEE Trans. Power Syst.*, vol. 30, no. 5, pp. 2665–2675, Sep. 2015.

[12] E. Ghahremani and I. Kamwa, "Dynamic state estimation in power system by applying the extended Kalman filter with unknown inputs to phasor measurements," *IEEE Trans. Power Syst.*, vol. 26, no. 4, pp. 2556–2566, Nov. 2011.

[13] S. Wang, W. Gao, and A. S. Meliopoulos, "An alternative method for power system dynamic state estimation based on unscented transform," *IEEE Trans. Power Syst.*, vol. 27, no. 2, pp. 942–950, May 2012.

[14] A. Khedher, N. Khemiri, and M. F. Mimouni, "Wind energy conversion system using DFIG controlled by backstepping and sliding mode strategies," *Int. J. Renew. Energy Res.*, vol. 2, no. 3, pp. 421–430, 2012.

[15] E. A. Wan and R. Van Der Merwe, "The unscented Kalman filter for nonlinear estimation," in *Proc. Adaptive Syst. for Signal Processing, Commun., and Control Symp. 2000 AS-SPCC*, Lake Louise, AB, Canada, Oct. 2000, pp. 153–158.

[16] E. Wan, "Sigma-point filters: an overview with applications to integrated navigation and vision assisted control," in *Proc. IEEE Nonlinear Statistical Signal Processing Workshop*, Cambridge, U.K., Sep. 2006, pp. 201–202.

[17] S. Das and T. Singh Sidhu, "Application of compressive sampling in synchrophasor data communication in WAMS," *IEEE Trans. Ind. Informat.*, vol. 10, no. 1, pp. 450–460, 2014.

[18] CERTS, Advanced Concepts faq, Jan. 2013 [Online]. Available: http://www.phasor-rtdms.com/phaserconcepts/phasor_adv_faq.html

[19] V. Akhmatov, *Induction Generators for Wind Power*. Brentwood, CA, USA: Multi-Science, 2005.

[20] A. Tapia, G. Tapia, J. X. Ostolaza, and J. R. Saenz, "Modeling and control of a wind turbine driven doubly fed induction generator," *IEEE Trans. Energy Convers.*, vol. 18, no. 2, pp. 194–204, Jun. 2003.

[21] K. Emami, T. Fernando, H. Iu, B. Nener, and K. Wong, "Application of unscented transform in frequency control of a complex power system using noisy PMU data," *IEEE Trans. Ind. Informat.*, to be published.

[22] S. J. Julier and J. K. Uhlmann, "New extension of the Kalman filter to nonlinear systems," in *Proc. Int. Soc. for Optics and Photonics (AeroSense'97)* , Orlando, FL, USA, Apr. 1997, pp. 182–193.

[23] I. Report, "Dynamic models for steam and hydro turbines in power system studies," *IEEE Trans. Power App. Syst.*, vol. PAS-92, no. 6, pp. 1904–1915, 1973.

[24] S. J. Julier and J. K. Uhlmann, "Unscented filtering and nonlinear estimation," *Proc. IEEE*, vol. 92, no. 3, pp. 401–422, Mar. 2004.

[25] S. J. Jul and J. K. Uhlmann, "New extension of the Kalman filter to nonlinear systems," in *Proc. Int. Soc. for Optics and Photonics (AeroSense'97)*, 1997, pp. 182–193.

Shenglong Yu (S'15) obtained his bachelor degree with honors in Measurement and Control Technology and Instrumentation from China University of Geosciences (Beijing) in 2011 and Master's degree of electrical and electronic engineering with distinction from the University of Western Australia in 2014. He is currently pursuing his Ph.D. degree at the University of Western Australia.

His research interests are in mathematical modeling of dynamical systems, functional observers, state estimation, power system analysis, renewable energy and control theories.

Kianoush Emami (M'15) obtained his bachelor and master of science in electrical engineering from Ferdowsi University of Mashhad, Iran in 1999 and 2002 respectively. Currently, he is pursuing his PhD degree at the University of Western Australia.

Between 2002 and 2006 he worked in the oil and gas industry as a control engineer and also as a project engineer. From 2006 to 2010 he joined Imamreza International University in Iran as a faculty member. His research interests are in functional observers, state estimation, control theory and power systems.

Tyrone Fernando (M'95–SM'05) obtained his bachelor of engineering with honours and the degree of doctor of philosophy from the University of Melbourne in 1990 and 1996 respectively.

In 1996 he joined the University of Western Australia, School of Electrical Electronic and Computer Engineering where he is currently a Professor. His research interests are in functional observers, state estimation, control theory, power systems and biomedical engineering.

Prof. Fernando has served as an Associate Editor for the IEEE TRANSACTIONS ON INFORMATION TECHNOLOGY IN BIOMEDICINE and also as guest editor for the journal of *Optimal Control Applications and Methods*.

Herbert Ho-Ching Iu (S'98–M'00–SM'06) received the B.Eng. (Hons) degree in electrical and electronic engineering from the University of Hong Kong, Hong Kong, in 1997. He received the Ph.D. degree from the Hong Kong Polytechnic University, Hong Kong, in 2000.

In 2002, he joined the School of Electrical, Electronic and Computer Engineering, The University of Western Australia where he is currently a Professor. His research interests include power electronics, renewable energy, nonlinear dynamics, current sensing techniques, and memristive systems.

Prof. Iu currently serves as a Guest Editor for the IEEE TRANSACTIONS ON INDUSTRIAL ELECTRONICS and several other journals including *IET Power Electronics*.

Kit Po Wong (M'87–SM'90–F'02) received the M.Sc, Ph.D., and D.Eng. degrees from the University of Manchester, Institute of Science and Technology, Manchester, U.K., in 1972, 1974, and 2001, respectively.

Since 1974, he has been with the School of Electrical, Electronic and Computer Engineering, the University of Western Australia, Perth, Australia, where he is currently a Winthrop Professor. His current research interests include power system analysis, planning and operations, and smart grids.

Prof. Wong received three Sir John Madsen Medals (1981, 1982, and 1988) from the Institution of Engineers Australia, the 1999 Outstanding Engineer Award from IEEE Power Chapter Western Australia, and the 2000 IEEE Third Millennium Award. He was Editor-in-Chief of *IEE Proceedings in Generation, Transmission and Distribution*. Currently he is serving as Editor-in-Chief for IEEE POWER ENGINEERING LETTERS.